Volume 13
Number 40
28 October 2025
Pages 20313–20792

Journal of Materials Chemistry C

Materials for optical, magnetic and electronic devices

rsc.li/materials-c

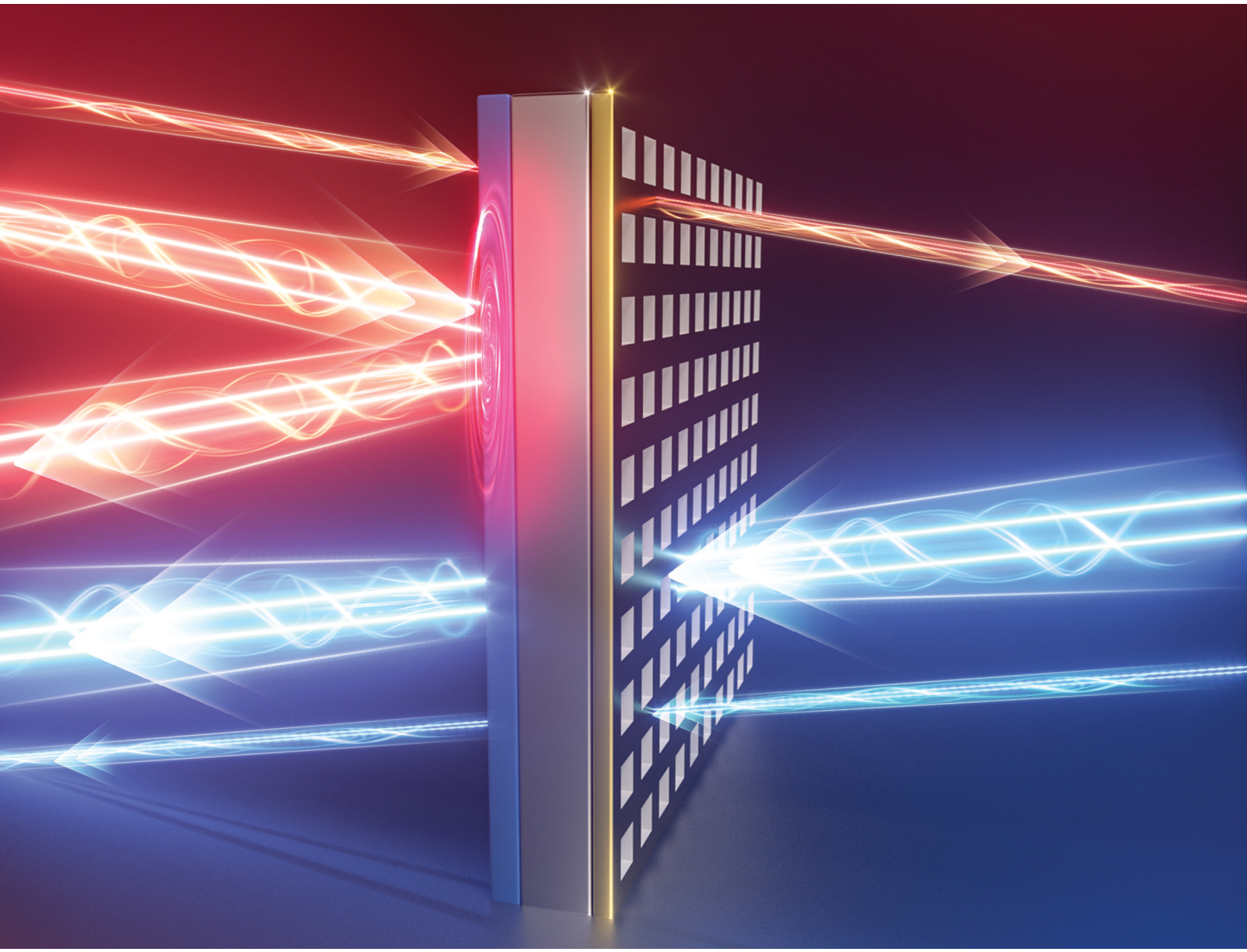

ISSN 2050-7526

ROYAL SOCIETY OF CHEMISTRY

PAPER

Yanlin Xu *et al.*

Self-activated nonreciprocal transmission isolation *via* absorption-asymmetry-triggered directional phase transition in VO_2-based terahertz metamaterials

Journal of Materials Chemistry C

ROYAL SOCIETY OF CHEMISTRY

PAPER

View Article Online
View Journal | View Issue

Cite this: J. Mater. Chem. C, 2025, 13, 20491

Self-activated nonreciprocal transmission isolation *via* absorption-asymmetry-triggered directional phase transition in VO_2-based terahertz metamaterials

Chenxi Liu, [a] Yanlin Xu, *[a] Hanqing Liu[a] and He Ma [b]

Received 4th August 2025,
Accepted 29th August 2025

DOI: 10.1039/d5tc02947c

rsc.li/materials-c

This study theoretically and numerically establishes a novel strategy for self-activated nonreciprocal transmission isolation in terahertz metamaterials, exploiting the absorption asymmetry of a vanadium dioxide (VO_2)-based structure to trigger directional phase transition under high-intensity illumination. Through coupled electromagnetic-thermal simulations, we analyze a tri-layer design where asymmetric absorption at specific frequencies—depending on incidence direction—induces markedly different thermal profiles. Crucially, high-intensity waves incident from the VO_2 side generate sufficient absorption-induced heating to surpass the phase transition threshold locally. This self-triggered phase change drastically suppresses transmission selectively for this direction, while waves incident from the opposing side experience significantly lower absorption and heating, maintaining high transmission. This fundamental asymmetry in thermal response enables nonreciprocal isolation without external excitation. Additionally, the transmission and absorption spectra are analyzed and the influences of absorption asymmetry, irradiation duration, incident power, and polarization direction are also investigated. This work demonstrates that harnessing absorption asymmetry to directionally control phase transition establishes a new paradigm for achieving nonreciprocal electromagnetic wave manipulation.

1. Introduction

Terahertz (THz) waves reside in the electromagnetic spectrum between traditional microwaves and far-infrared region. Terahertz radiation exhibits a superior transmission bandwidth and higher imaging resolution than microwaves, while retaining greater penetration depth than optical waves.[1] Due to potential applications in fields such as non-destructive testing, high-speed communication, radar remote sensing, and material detection, terahertz technology has attracted extensive attention and achieved rapid development in the past decade.[2–4] Nevertheless, naturally occurring materials demonstrating robust electromagnetic interactions with THz waves are exceptionally scarce. This inherent challenge has stimulated intensive research into artificially structured composites capable of overcoming material-level restrictions. Metamaterials, characterized by rationally designed subwavelength geometries, are emerging as promising candidates for THz wave manipulation. The technological advancement of the metamaterial is poised to accelerate deployment of THz systems in potential application scenarios.

Metamaterials, implemented as the subwavelength resonator array, can achieve desired electromagnetic manipulation through specialized design.[5–7] In particular, metamaterial-based absorbers, modulators, and switches have attracted extensive research attention.[8–12] Integrating materials with unique electromagnetic properties into metamaterials introduces new degrees of freedom for electromagnetic control, thereby enhancing their functionality. Common active materials or devices include graphene, liquid crystals, MXene, phase-change materials, micro-electro-mechanical systems (MEMS) and so on.[13–17] For example, Zhang *et al.* proposed a graphene-based metamaterial absorber that achieves tunable broadband terahertz absorption by varying the Fermi level.[18] Utilizing MEMS technology featuring electrostatically actuated membranes, Liu *et al.* realized an ultrathin tunable terahertz absorber demonstrating capabilities in fast switching, resonant frequency shifting, and significant absorption modulation.[19] Despite the incorporation of various functional materials, achieving non-reciprocal transmission characteristics is challenging. Non-reciprocal transmission is crucial for applications like unidirectional isolation, limiting, and reverse clutter suppression.[20–24] Recently, the design of metamaterials for non-reciprocal transmission has attracted more

[a] College of Electronic Science and Technology, National University of Defense Technology, Changsha, 410073, China. E-mail: ylxu0724@nudt.edu.cn
[b] College of Science, Beijing University of Technology, Beijing, 100124, China

and more interests. Existing reported studies primarily focus on utilizing chiral design to achieve asymmetric polarization conversion.[25–27] For instance, Huang *et al.* employed graphene-based chiral metamaterials and complementary structures to achieve circular polarization conversion and tunable asymmetric transmission in the terahertz band. However, this approach does not provide completely unidirectional isolation for incident waves because the electromagnetic energy is still mainly transmitted and only the polarization direction has been changed. Researches on optical metamaterials mainly utilizes magnetically biased gyrotropic materials to generate asymmetric permittivity tensors for transmission control.[28,29] While in microwave regime, researchers have explored using externally biased nonlinear diodes or amplifiers to achieve asymmetric transmission.[30,31] These metamaterial structures are commonly complex and rely on auxiliary excitation setups dependent on the wave propagation direction.

This work proposes a VO_2-based terahertz metamaterial featuring non-reciprocal characteristics under high-intensity illumination, while also simultaneously achieving tunable, polarization-insensitive wave transmission and absorption. The unit cell of the designed structure consists of a simple metallic square ring, a silicon dielectric substrate, and a VO_2 film. When VO_2 is insulating, unlike conventional metamaterial absorbers with metallic plane, the proposed structure maintains significant transmission capabilities while exhibiting moderate multi-frequency absorption performance. Upon phase transition of the VO_2 layer, terahertz transmission is nearly completely suppressed, and a distinct absorption peak emerges when terahertz radiation illuminates the metallic-ring side. It is worthy to note that the structure consistently exhibits asymmetric absorption characteristics regardless of the phase state in VO_2 layer. Particularly, a pronounced discrepancy in absorption between different incidence side occurs at the third absorption peak when VO_2 is in insulating phase. Through electromagnetic-thermal co-simulation, we analyse the thermal responses arising from absorption-dissipated under high-intensity illumination from different side. Interestingly, it can be found that the asymmetric absorption characteristics lead to differential heating of the metamaterial. The temperature difference between two scenarios induces a directionally-dependent phase transition, which in turn gives rise to the non-reciprocal transmission properties of incident waves. For comparison, this nonreciprocal phenomenon cannot be observed in the condition when absorption exhibits minimal divergence for illumination from different side.

2. Design and method

2.1. Structural design

The schematic metamaterial design and the unit cell is depicted in Fig. 1. The unit cell of the metamaterial is a three-layer sandwich structure with square shape. The top layer features a metallic square ring structure, which provides electromagnetic resonance. The fourfold rotational symmetry of the square-ring resonator inherently ensures polarization-independent responses.

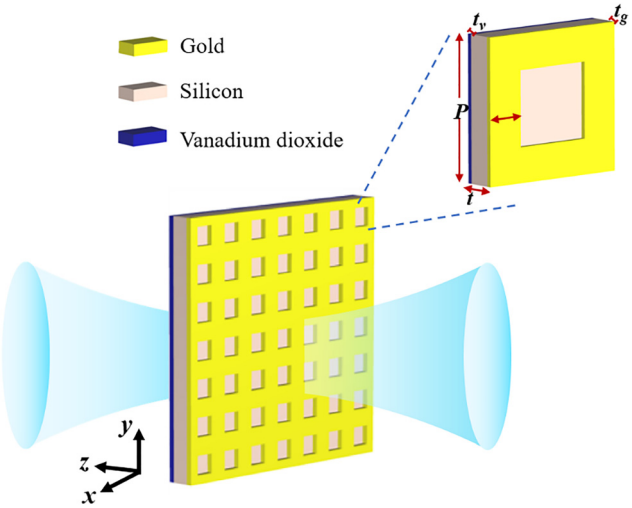

Fig. 1 Schematic illustration of proposed metamaterial and its unit cell. The *y*-polarized terahertz radiation transmitted through the metamaterial along *z* direction.

The intermediate dielectric layer is made of silicon substrate, chosen for its compatibility with standard microfabrication techniques and well-characterized dielectric properties. The inherent loss tangent ($\tan\delta = 2.5 \times 10^{-4}$) introduces electromagnetic dissipation, which may enhance the wave absorption. The bottom layer employs phase-change VO_2 instead of a metallic reflector. Thus, when VO_2 is in the insulating state, this design allows good terahertz transmission. The periodic length of the unit cell P is 60 μm. The top metallic square ring has a width w = 13 μm and a thickness of t_g = 200 nm, fabricated from gold with an electrical conductivity of 4.5×10^7 S m^{-1}. The silicon dielectric layer is t = 25 μm thick, with a relative permittivity of 11.9. The bottom layer is a VO_2 film with the thickness t_v = 500 nm.

2.2. Simulation model

In terahertz region, the dielectric constants of the VO_2 film can be described using Drude model.[32–34]

$$\varepsilon(\omega) = \varepsilon_\infty - \frac{\omega_p^2(\sigma)}{\omega^2 + i\gamma\omega} \quad (1)$$

$$\omega_p^2(\sigma) = \frac{\sigma}{\sigma_0}\omega_p^2(\sigma_0) \quad (2)$$

where σ is the conductivity of VO_2, ε_∞ = 12 is dielectric permittivity at infinite frequency, $\omega_p(\sigma) = 1.4 \times 10^{15}$ rad s^{-1} is plasma frequency, $\gamma = 5.75 \times 10^{13}$ rad s^{-1} is the collision frequency, $\sigma_0 = 3 \times 10^5$ S m^{-1}, $\omega_p(\sigma_0) = 1.5 \times 10^{15}$ rad s^{-1}. The conductivity of the insulating VO_2 is set as 200 S m^{-1} while when it undergoes phase transition to the metallic state, the conductivity is increased to 200 000 S m^{-1} with three-order-of-magnitude variation which is relatively feasible to achieve in practical applications.

The electromagnetic characteristics of the metamaterial are simulated using CST Microwave Studio, focusing on the 1.7–2.4 THz frequency range. Periodic boundary conditions are applied along the *x*- and *y*-axes of the unit cell, while an open

boundary condition is set along the z-axis. Terahertz waves initially polarized in y direction are incident perpendicularly onto the metamaterial surface along the z-direction. The transmission (T), reflection (R), and absorption (A) coefficients can be calculated from the simulated S-parameters results, where $T = |S_{21}|^2$, $R = |S_{11}|^2$, and the absorption can be derived form $A = 1 - R - T$.

3. Results and discussion

3.1. Transmission and absorption characteristics

Fig. 2(a) depicts the transmission and reflection curves of the metamaterial under terahertz incidence from the metallic square ring layer side and the VO_2 layer side respectively when VO_2 is in insulating phase. It can be observed that the transmission curves coincide regardless of the incidence direction, confirming the reciprocal feature of terahertz propagation. Distinct transmission peaks emerge near 1.84, 2.11, and 2.35 THz, with the third peak exhibiting slightly lower intensity than the lower-frequency counterparts. Correspondingly, the reflection curves display valleys at these three frequencies. It is evident that the two reflection curves do not overlap: incidence from the VO_2 side yields notably lower reflection dips at the second and third frequencies compared to metallic side incidence, indicating direction-dependent absorption at these bands. Fig. 2(b) illustrates the absorption spectra for both incidence directions, featuring three unnegligible peaks at the same frequencies as above.

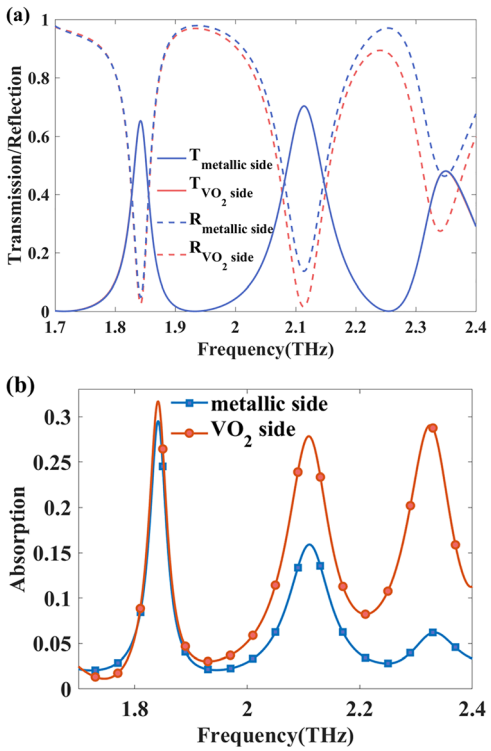

Fig. 2 (a) Transmission, reflection and (b) absorption coefficients as terahertz waves are incident on the metamaterial from the metal square ring side and the VO_2 side respectively when VO_2 is in insulating phase.

The maximum absorption efficiency is moderate ($\approx$0.3), but significant directional disparities are observed: while absorption differences are slight at the first frequency, they become pronounced at the latter two frequencies. This behavior highlights the structure's anisotropic absorption response to electromagnetic waves incident from different directions.

To analyze the mechanism of the electromagnetic response, the electric field distributions and power loss densities are simulated at 1.84, 2.11, and 2.35 THz, when terahertz waves illuminates on the metamaterial from the side of the metal square ring. As can be seen from Fig. 3(a)–(c), the electric field intensities on both sides of the metamaterial are comparable in magnitude, indicating that the terahertz waves exhibit good transmission at all three frequencies. The field intensities inside the metamaterial show significant discrepancies, which stems from differences in resonance generation. The power loss densities depicted in Fig. 3(d)–(f) reveal that the primary loss during wave transmission occurs in the VO_2 layer. It is observed that the loss density is highest at 1.84 THz, followed by 2.11 THz, and significantly lower at 2.35 THz. This frequency-dependent loss density exactly matches the trend of absorption intensity, where the absorption peak at 1.84 THz exceeds those at 2.11 THz and 2.35 THz. Furthermore, to explain the response under different incident directions, Fig. 3(g)–(i) illustrate the power loss densities at the three frequencies when terahertz waves are incident from the VO_2 side. Notably, the power loss densities in the VO_2 layer at 2.11 THz and 2.35 THz are significantly higher than those when the metamaterial is under metal square ring-side incidence. This discrepancy in loss densities accounts for the absorption-asymmetry characteristics of the structure under

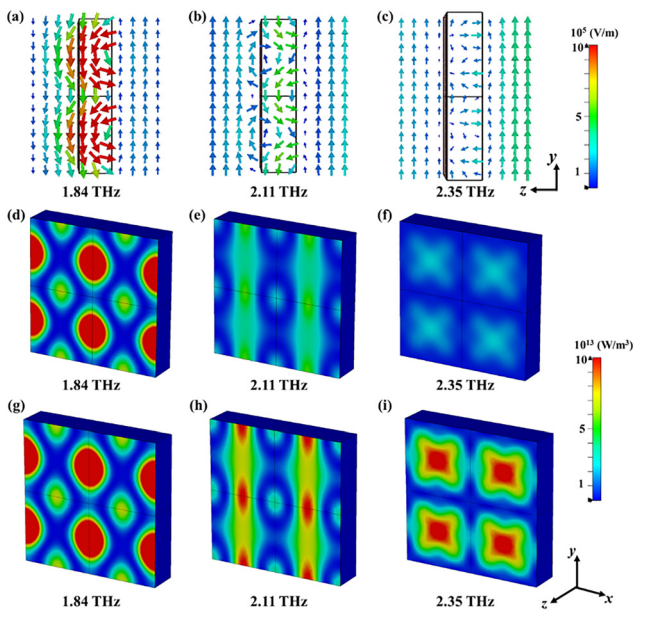

Fig. 3 (a)–(c) Electric field distributions at different frequencies when terahertz waves are incident on the metamaterial from the metallic square ring side. Power loss density in the metamaterial for incidence (d)–(f) from the metallic ring side and (g)–(i) from the VO_2 side at different frequencies.

different incidence directions. The difference in absorption stems from the distinct electromagnetic responses of the materials in their respective states. The metallic side exhibits high reflectivity due to its excellent electrical conductivity, leading to lower absorption. In contrast, the VO_2 side, particularly when in its insulating state, allows greater wave penetration and energy dissipation within the material, resulting in higher absorption.

When the VO_2 film transitions to the metallic phase, the transmission characteristics of the metamaterial exhibit significant changes. As shown in Fig. 4(a), the transmission and reflection spectra demonstrate that terahertz waves show negligible transmission through the metamaterial structure regardless of the incident direction. This arises because the VO_2 film acts analogous to the metallic reflective surface of a conventional absorber. The reflection curves display distinct features: terahertz waves incident from the VO_2 side maintain high reflection across the entire frequency range, whereas waves incident from the metal square ring side exhibit a reflection valley at 2.01 THz. This disparity is further reflected in the absorption curve of Fig. 4(b), where a pronounced absorption peak up to 0.74 is observed exclusively under metal square ring-side incidence. This absorption value exceeds the three absorption peaks recorded in the insulating state.

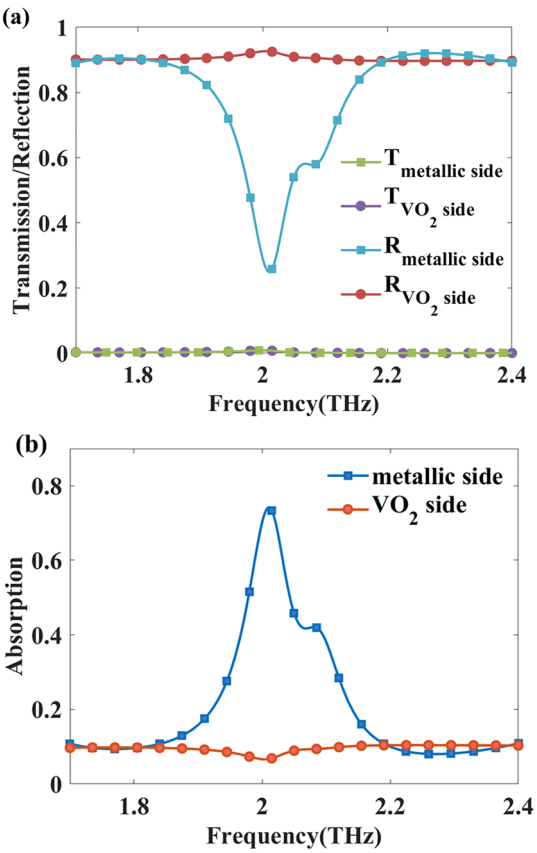

Fig. 4 (a) Transmission, reflection and (b) absorption coefficients as terahertz waves are incident on the metamaterial from the metal square ring side and the VO_2 side respectively when VO_2 is in metallic phase.

From the above analysis, it is evident that the transmission characteristics of electromagnetic waves exhibit substantial alterations when VO_2 is in metallic phase compared to the insulating phase. Further, we analyze the modulation effects induced by the phase transition of VO_2. Generally, the modulation depth (MD) is adopted to quantify the terahertz modulation capability, expressed as: $MD = |T_{in} - T_{me}|/T_{in}$. Here, T_{in} denotes the transmission coefficient of VO_2 in the insulating phase, and T_{me} represents that in the metallic phase. Calculations reveal that the modulation depths at 1.84, 2.11, and 2.35 THz reach as high as 99.5%, 99.8%, and 99.9%, respectively. Such extremely high modulation depths arise from the near-complete transmission cutoff at these frequencies when VO_2 is in metallic phase, exhibiting almost switching performances. The modulation depth curve is not provided here. This is because transmission coefficients outside the transmission band are remarkably low for VO_2 both in its insulating phase and metallic state, which could lead to anomalously large values in MD calculations. However, since wave transmission is virtually impossible under these conditions, the practical significance of such calculation results is limited. It should be noted that the incident direction of electromagnetic waves is not considered in modulation analysis, as electromagnetic wave transmission is reciprocal, ensuring consistent results regardless of the incident direction.

Furthermore, we employ the impedance matching principle to investigate the wave absorption characteristics of the metamaterial when VO_2 is in the metallic state. When the metamaterial's impedance is well-matched to free space, terahertz waves can enter the structure with minimal reflection then the resonance effects occurred within the metamaterial induce the power dissipation. The equivalent medium impedance of the metamaterial can be extracted from the *S*-parameters using the following formula: [35–37]

$$Z = \frac{\sqrt{(1+S_{11})^2 - S_{21}^2}}{\sqrt{(1-S_{11})^2 - S_{21}^2}}$$

The real and imaginary parts of the equivalent medium impedance were calculated. Since this is the normalized impedance, the metamaterial should exhibit a numerical impedance close to 1 when matched to free space. As shown in Fig. 5(a), near the absorption peak at 2.01 THz, the imaginary part of the equivalent impedance approaches zero, while the real part is slightly greater than 1. This indicates good impedance matching with free space which results in minimal interface reflection and thus forming a pronounced absorption peak. Similarly, the equivalent impedance is also calculated when terahertz waves are incident from the VO_2 side. As depicted in Fig. 5(b), although frequency points exist where the imaginary part of the impedance approaches zero across the entire band, the real part of the impedance significantly deviates from 1. Consequently, the impedance matching between air and the VO_2 film interface is poor, causing strong reflection and the absence of obvious wave absorption.

As is observed, the metamaterial structure proposed in this work enables both modulation and wave absorption

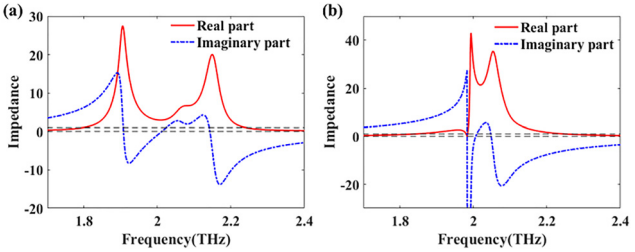

Fig. 5 Normalized effective medium impedance curve of the metamaterial as terahertz waves are incident from (a) the metallic square ring side and (b) the VO_2 side respectively when VO_2 is in metallic state.

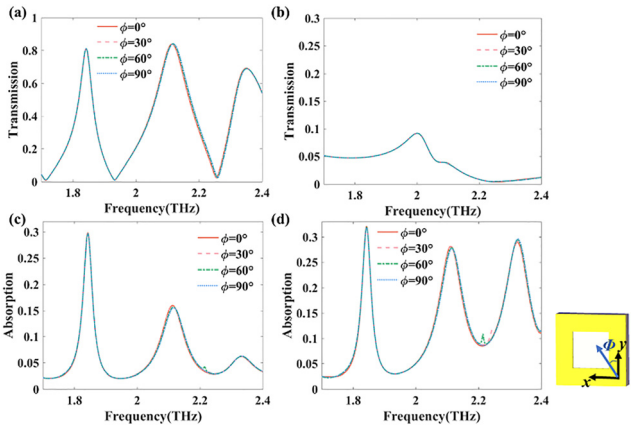

Fig. 6 Transmission curves with the polarization angle increasing from 0° to 90° (a) before and (b) after phase transition. Absorption characteristics as a function of polarization angles under illumination from (c) the metallic square ring side and (d) the VO_2 side respectively when VO_2 is in insulating phase.

capabilities. For practical applications, the adaptability to different polarization angles also needs to be considered. Here, we analyze the influence of polarization angles on its transmission characteristics. Fig. 6(a) and (b) present the transmission curves with the polarization angle increasing from 0° to 90° before and after phase transition, respectively. It can be found that the positions and magnitudes of the transmission peaks remain highly consistent, showing invariable modulation performance resulting from the phase transition regardless of the polarization directions. Similarly, Fig. 6(c) and (d) illustrate the absorption characteristics as a function of polarization angles under illumination from the metallic square ring side and the VO_2 side respectively when VO_2 is in insulating phase. The absorption curves also exhibit excellent consistency with changing polarization angles, with no shifts in peak positions or absorption rates. This indicates the asymmetric wave absorption is also insensitive to the polarization direction. The polarization-independent behavior is primarily attributed to the high structural symmetry of the metamaterial architecture.

3.2. Nonreciprocal transmission isolation *via* directional phase transition

It is worthy to mention that the transmission of the metamaterial remains reciprocal regardless of whether VO_2 is in the insulating or metallic phase. In contrast, the reflection or absorption curves exhibit variations depending on the incident side. Here, we propose that absorption nonreciprocity can be leveraged to construct transmission nonreciprocity. By establishing specific "absorption-asymmetry-triggered" conditions, absorption-asymmetry induces direction-dependent modifications in the medium's properties, thereby enabling nonreciprocal electromagnetic transmission. The coupling condition we implement is high-intensity incident fields. When the incident terahertz intensity is sufficiently high, its absorption may cause temperature changes in the metamaterial which may trigger the phase transition of VO_2 *via* the thermal effect. Due to the intrinsic nonreciprocal absorption, waves with identical field strength but from opposite illumination directions do not lead to the phase transition critical temperature simultaneously. Consequently, at certain field intensity, electromagnetic waves incident from different sides exhibit distinctive transmission curves corresponding to insulating and metallic states of VO_2 respectively.

Temperature is a critical factor determining whether the VO_2 undergoes a phase transition. Thus, we investigate the temperature variation of the metamaterial under high-intensity terahertz incidence. The temperature evolution of the designed metamaterial is analyzed using electromagnetic-thermal coupled simulation which can be carried out using CST software. In our calculation, specific heat capacity, heat conductivity coefficient, density of the insulating VO_2 are set as 0.656 kJ K^{-1} kg^{-1}, 3.5 W K^{-1} m^{-1}, and 4.57 g cm^{-3}, respectively. The values are changed to 0.78 kJ K^{-1} kg^{-1}, 6 W K^{-1} m^{-1}, and 4.64 g cm^{-3} for metallic state respectively.[38] The specific heat capacity, heat conductivity coefficient, density of silicon substrate are set as 0.7 kJ K^{-1} kg^{-1}, 148 W K^{-1} m^{-1}, and 2.33 g cm^{-3}. While these parameters of metal gold are set as 0.13 kJ K^{-1} kg^{-1}, 314 W K^{-1} m^{-1}, and 19.32 g cm^{-3}. During the simulation, we first employ electromagnetic modeling to obtain the field distribution, current distribution, and loss distribution for electromagnetic-thermal coupled analysis. Then, thermal simulation is performed to characterize the temperature variation of the metamaterial. In the simulation, the ambient temperature is uniformly set at 293.15 K (20 °C). Given the periodic array structure adopted in the metamaterial design, thermal insulation boundaries are specified for the *x*- and *y*-direction boundaries of each unit cell. Open boundary conditions are implemented for the *z*-direction to simulate unbounded spatial propagation.

When illuminated by high-intensity terahertz waves, the transmission characteristics of the designed metamaterial can be categorized into three scenarios. In the first scenario, the terahertz waves incident from both sides fail to raise the temperature of the metamaterial sufficiently to trigger the phase transition of VO_2, which remains in insulating state. Therefore, the transmitted waves exhibit low attenuation, enabling efficient transmission regardless of the incident side. In the second scenario, terahertz waves from both sides raise the temperature of the metamaterial beyond the VO_2 phase transition threshold, leading to high attenuation and blocking of transmission from either direction. The third scenario

occurs when the temperature rise induced by incident waves from one side exceeds that from the other, such that the temperature difference range encompasses the phase transition critical temperature of VO_2. This creates a condition when terahertz waves can transmit through one side (VO_2 remains insulating) but are blocked by the other side (VO_2 undergoes phase transition), thereby achieving non-reciprocal transmission for the same incident condition. This specific scenario constitutes the primary focus of our study.

To investigate the non-reciprocal transmission characteristics under high-intensity terahertz incidence from different side, we selected the third scenario with the maximum absorption discrepancy circumstance. As shown in Fig. 2(b), the absorption rate difference at 2.35 THz reaches approximately 0.24 for opposite incidence directions, making this frequency point the focus of our study on high-intensity electromagnetic responses of the metamaterial. Fig. 7(a) and (b) depict the temperature distributions 1 s after terahertz waves are incident on the metamaterial surface from the metal square ring side and VO_2 side, respectively. The incident electric field strength in the simulation is set to 100 V cm^{-1}. It is worthy to note that when waves are incident from the metal square ring side, the temperature reaches to 323 K—substantially below the typical phase transition threshold (≈68 °C, 341.15 K), thus the phase transition is unlikely to occur. The wave transmission in this case aligns with the pattern shown in Fig. 2(a). Conversely, incidence from the VO_2 side causes a significant temperature to rise to 414 K, far exceeding the phase transition threshold. This triggers the phase transition of VO_2 layer, altering the transmission characteristics to the state depicted in Fig. 4(a), thereby achieving a non-reciprocal transmission isolation as shown in Fig. 7(c). We can quantify the degree of non-reciprocity by the difference in the transmission coefficient (in dB) between the two illumination directions. As can be calculated, the non-reciprocity levels at the three frequencies of 1.84, 2.11, and 2.35 TH reach 24 dB, 28 dB, and 37 dB, respectively. These results indicate that at these frequencies, the terahertz wave can effectively transmit when incident from the metal square ring side, whereas it is significantly blocked when incident from the VO_2 side.

The high-intensity wave incidence condition should be particularly emphasized. This is because when the incident field strength is low, the thermal loss generated by wave absorption is insufficient to significantly increase the temperature of the metamaterial. For instance, when the incident wave field strength in the simulation is reduced by an order of magnitude to 10 V cm^{-1}, the maximum temperature of the metamaterial at 1 s after terahertz incidence from both sides remains below 295 K, showing no significant difference from the ambient temperature. Certainly, if the incident field strength is excessively high, there may be a situation where the temperature becomes extremely high for both incident directions. For instance, when the field strength is 1000 V cm^{-1}, the simulated temperature of the metamaterial exceeds 600 K after 1 s. Obviously, in this case, VO_2 will undergo phase transition regardless of the incident side. Therefore, the non-reciprocal transmission of metamaterials is conditional on a range of incident field strengths.

It should also be emphasized that such nonreciprocity occurs at frequencies where noticeable absorptive nonreciprocity is present. As a contrast, we investigated the temperature rise of the metamaterial at 1.84 THz, which corresponds to the first transmission peak. As shown in Fig. 2(b), the difference in absorption when terahertz waves are incident from the metal square side and VO_2 side at this frequency is slight, with a value of approximately 0.02. In the simulation, all setup parameters except the frequency are kept the same as those used in previous calculations. Fig. 8(a) and (b) present the temperature distributions when terahertz waves are incident from different side. It is evident that the temperature increases in the two cases are quite similar, reaching 451 K and 462 K, respectively. This indicates that at this frequency, waves incident from either side can induce the phase transition of VO_2, which corresponds to the second scenario analyzed above. After the phase transition, the incident waves are isolated with large loss, but the transmission performance still remains reciprocal.

Since a continuous wave incidence condition is utilized, the impact of incidence time must be considered, as the heat

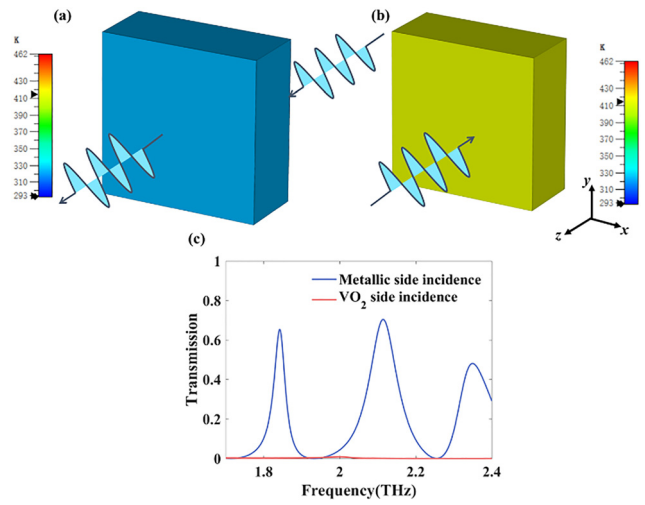

Fig. 7 Temperature distributions of the metamaterial 1 s after terahertz waves at 2.35 THz are incident on the metamaterial surface from (a) the metal square ring side and (b) the VO_2 side, respectively. (c) Non-reciprocal transmission isolation when high-intensity terahertz wave illuminates on the metamaterial from different side.

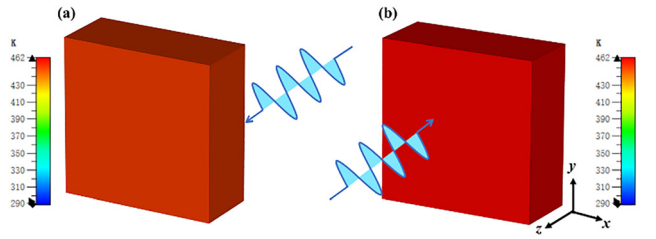

Fig. 8 Temperature distributions of the metamaterial 1 s after terahertz waves at 1.84 THz are incident on the metamaterial surface from (a) the metal square ring side and (b) the VO_2 side, respectively.

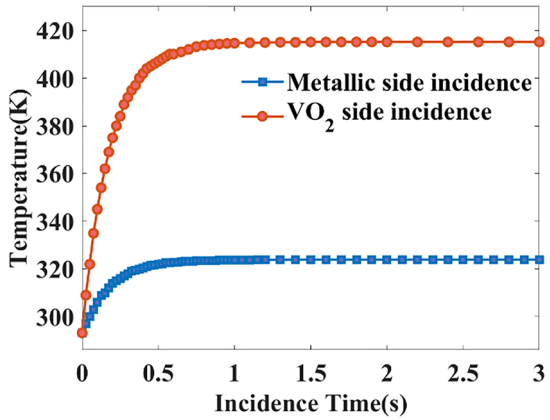

Fig. 9 Time-dependent temperature variation of the metamaterial when irradiated by high-intensity terahertz waves from the metallic square ring side and the VO_2 side for duration time of 3 s.

generated by electromagnetic losses may accumulate. This implies that the temperature of the metamaterial may gradually increase with the prolongation of the incidence time. Specifically, the transient temperatures of the metamaterial are simulated when the high-intensity terahertz waves are incident from the different sides. The total simulation duration was set to 3 seconds with a default time interval of 100 ms. To accurately capture the rapid changes during the initial transient phase, the time step was reduced to 25 ms for the first 500 ms of the simulation. As shown in Fig. 9, regardless of the incidence side, the metamaterial temperature first increases with time and then nearly reaches a saturation state without significant change, which can be attributed to the heat dissipation. When the metamaterial temperature rises above the ambient temperature, heat dissipation balances the heat generation. The saturation temperatures in the two cases are 324 K and 415 K, showing no obvious difference from the temperature at duration time of 1 s. This indicates that even with prolonged illumination, the high-intensity waves incident from the metal square ring side are unlikely to induce the phase transition of VO_2.

It is worthy to note that an infinitely large periodic structure is assumed in our simulation. As such, adiabatic boundary conditions were applied in the thermal simulations, which assume uniform heat generation in the surrounding environment and no heat dissipation in the x- and y-directions. In practical finite-sized scenarios, however, heat dissipation will inevitably occur at the boundaries of the metamaterial array as the temperature exceeds the ambient level, ultimately leading to a reduction in the overall temperature of the structure. This implies that the temperatures obtained from the calculations may be higher than those expected in practical applications. Despite this potential temperature discrepancy, the simulation results still demonstrate that under specific high-intensity incidence conditions, asymmetric wave absorption will lead to direction-dependent phase transition, giving rise to the non-reciprocal transmission isolation.

The ''absorption-asymmetry-triggered'' approach to achieve non-reciprocal characteristics proposed in our work can be adapted to a broader range of applications by changing the structure and materials. For example, by modifying the structural dimensions, this non-reciprocal characteristic may be realized in both microwave and optical frequency bands. Moreover, through improved structural design, greater differences in wave absorption can be realized at specific frequencies. This enlargement can ensure that the temperature interval between the two incident conditions encompasses the phase transition critical point of VO_2 over a wider range of incident field strengths, thereby resulting in non-reciprocal transmission. Meanwhile, VO_2 used in this study is merely a typical example; other phase-change materials with transition temperatures tailored to specific needs can be employed. Furthermore, since there is no discernible difference in absorption across varying polarization angles as shown in Fig. 4, it is evident that this non-reciprocal transmission characteristic is insensitive to the polarization of the incident high-intensity terahertz waves. Additionally, this non-reciprocal transmission determined by the field intensity occurs adaptively without the application of any auxiliary measures. From the view of application, this non-reciprocal transmission under high-intensity illumination can be applied in scenarios such as electromagnetic isolators and limiters.

Specifically, subsequent studies may focus on the possible terahertz-field-induced phase transitions in the VO_2-based metamaterial using simulation modeling and analytical methods. This research concerns characterizing the relationship between field enhancement, localized power dissipation, and the critical electric field required for field-induced phase transition. Relevant analysis may also be conducted to understand how absorption asymmetry governs the spatial progression of directional phase transitions.

4. Conclusion

This study presents a strategy for achieving nonreciprocal transmission *via* absorption-asymmetry-triggered directional phase transition in VO_2-based terahertz metamaterials, simultaneously realizing tunable transmission and absorption properties. By simulating high-intensity incidence conditions, we exploit absorption asymmetry to achieve directional phase transition resulting in the nonreciprocal transmission isolation, which has never been reported to the best of our acknowledge. The metamaterial features a simple tri-layer structure comprising metallic square rings, a silicon dielectric substrate, and a VO_2 layer. Simulations reveal three distinct absorption peaks in the terahertz range when VO_2 is in insulating state at room temperature, accompanied by moderate absorption at corresponding frequencies. Crucially, we separately investigated wave incidence from the metallic ring side and VO_2 side. While transmission coefficients remain reciprocal under both illumination directions, significant absorption differences emerge. At 1.84 THz absorption peak, the absorption asymmetry is minimal, whereas at 2.35 THz, the absorption coefficient difference reaches 0.24. As VO_2 undergoes transition to the metallic phase,

both transmission and absorption characteristics are modulated. The transmission maintains reciprocity showing electromagnetic isolation for either incidence side but the absorption turns to be more nonreciprocal—a prominent absorption peak persists only for incidence from the metallic ring side. Employing the absorption asymmetry the directionally-triggered phase transition mechanism is established to realize nonreciprocal transmission isolation. Through electromagnetic-thermal simulations under high-intensity radiation 100 V cm^{-1}, we demonstrate that illumination exclusively from the VO_2 side generates sufficient heat to exceed the phase transition threshold. Consequently, VO_2-side incidence triggers insulator-to-metallic transition leading to the transmission suppression, while irritation from metallic square ring side maintains high transmission without phase transition—enabling nonreciprocal transmission isolation. Conversely, at 1.84 THz where absorption asymmetry is merely 0.02, bidirectional illumination induces comparable temperature rises that both exceed the phase transition threshold. This results in symmetric transmission isolation for both incidence directions, still maintaining reciprocal characteristics. The effect of field intensity, duration, and polarization directions are also investigated. This architecture permits functional customization through geometric/material modification, showing promising potential for nonreciprocal optical limiters, isolators, controllable absorber as well as transmission modulators.

Author contributions

Chenxi Liu: conceptualization, methodology, major design and simulation, data curation, writing—original draft, and writing – review & editing. Yanlin Xu: design and simulation, conceptualization, and data curation. Hanqing Liu: data curation. He Ma: supervision and validation.

Conflicts of interest

The authors declare that they have no known competing financial interests or personal relationships that could have appeared to influence the work reported in this paper.

Data availability

The data supporting this article are available from the article content.

Acknowledgements

This work is supported by the National Natural Science Foundation of China (62293491).

References

1 T. Nagatsuma, G. Ducournau and C. C. Renaud, Advances in terahertz communications accelerated by photonics, *Nat. Photonics*, 2016, **10**(6), 371–379.
2 P. H. Siegel, Terahertz technology, IEEE Trans, *Microwave Theory Tech.*, 2002, **50**, 910–928.
3 Y.-S. Lin, S. Liao and X. Liu, Tunable terahertz metamaterial by using three-dimensional double split-ring resonators, *Opt. Laser Technol.*, 2019, **112**, 215–221.
4 F. Lu, H. Ou and Y.-S. Lin, Reconfigurable terahertz switch using flexible L-shaped metamaterial, *Opt. Lett.*, 2020, **45**(23), 6482–6485.
5 H. T. Chen, W. J. Padilla, J. M. O. Zide, A. C. Gossard, A. J. Taylor and R. D. Averitt, Active terahertz metamaterial devices, *Nature*, 2006, **444**, 597–600.
6 X. Shi, H. Lin, T. Liu, Y. Shen, R. Tang, L. Li, J. Zhang, Y. Wu, S. Duan, C. Zhao and S. Xiao, Polarization-controlled non-Hermitian metasurfaces for ultra-sensitive terahertz sensing, *Laser Photonics Rev.*, 2025, **19**(14), 2500172.
7 B. X. Wang, G. Y. Duan, W. Z. Lv, Y. Tao, H. Xiong, D. Q. Zhang, G. F. Yang and F. Z. Shu, Design and experimental realization of triple-band electromagnetically induced transparency terahertz metamaterials employing two big-bright modes for sensing applications, *Nanoscale*, 2023, **15**, 18435–18446.
8 D. Wang, K. D. Xu, S. Luo, Y. Cui, L. Zhang and J. Cui, A high Q-factor dual-band terahertz metamaterial absorber and its sensing characteristics, *Nanoscale*, 2023, **15**, 3398–3407.
9 J. Ge, Y. Zhang, H. Dong and L. Zhang, Nanolayered VO_2-based switchable terahertz metasurfaces as near-perfect absorbers and antireflection coatings, *ACS Appl. Nano Mater.*, 2022, **5**(4), 5569–5577.
10 H. Zhu, Y. Zhang, L. Ye, Y. Li, Y. Xu and R. Xu, Switchable and tunable terahertz metamaterial absorber with broadband and multi-band absorption, *Opt. Express*, 2020, **28**, 38626–38637.
11 T. Zhou, P. Liu, C. Liu, H. Jiang and T. Tian, Multilayer energy selective surface with wide operational band and high shielding effectiveness based on second-order filter, *IEEE Trans. Electromag. Compat.*, 2025, **67**(1), 337–340.
12 S. Xiao, T. Wang, T. Liu, X. Yan, Z. Li and C. Xu, Active modulation of electromagnetically induced transparency analogue in terahertz hybrid metal-graphene metamaterials, *Carbon*, 2019, **126**, 271–278.
13 M. Manjappa, P. Pitchappa, N. Wang, C. Lee and R. Singh, Active control of resonant cloaking in a terahertz MEMS metamaterial, *Adv. Opt. Mater.*, 2018, **6**, 1800141.
14 J. M. Ngobeh, V. Sorathiya, A. Alwabli, A. Y. Jaffar and O. S. Faragallah, MXene based multilayered and ultrawideband absorber for solar cell and photovoltaic applications, *Sci. Rep.*, 2015, **15**(1), 1–17.
15 H. Hu, H. Zhang, H. Jiang, Z. Cui, Y. Wang and D. Wu, Tunable multifunctional terahertz metamaterial device based on metal-dielectric-vanadium dioxide, *Opt. Laser Technol.*, 2025, **181**, 111629.
16 S. Savo, D. Shrekenhamer and W. J. Padilla, Liquid crystal metamaterial absorber spatial light modulator for THz applications, *Adv. Opt. Mater.*, 2014, **2**(3), 275–279.
17 Y. K. Srivastava, A. Chaturvedi, M. Manjappa, A. Kumar, G. Dayal, C. Kloc and R. Singh, MoS_2 for ultrafast all-optical

switching and modulation of THz Fano metaphotonic devices, *Adv. Opt. Mater.*, 2017, **5**(23), 1700762.

18 K. Zhang, S. Dong, X. Wu, K. Yu and Y. Liu, Graphene-based tunable broadband metamaterial absorber for terahertz waves, *Opt. Laser Technol.*, 2025, **180**, 111490.

19 M. Liu, M. Susli, D. Silva, G. Putrino, H. Kala, S. Fan, M. Cole, L. Faraone, V. P. Wallace, W. J. Padilla, D. A. Powell, I. V. Shadrivov and M. Martyniuk, Ultrathin tunable terahertz absorber based on mems-driven metamaterial, *Microsyst. Nanoeng.*, 2017, **3**, 17033.

20 T. Lou, X.-X. Yang, G. He, W. Che and S. Gao Dual-polarized, nonreciprocal spatial amplification active metasurface, *IEEE Antennas Wirel. Propag. Lett.*, 2021, **20**(9), 1789–1793.

21 W. Yang, J. Qin, J. Long, J. Long, W. Yan, Y. Yang, C. Li, E. Li, J. Hu, L. Deng, Q. Du and L. Bi, A self-biased nonreciprocal magnetic metasurface for bidirectional phase modulation, *Nat. Electron.*, 2023, **6**, 225–234.

22 Y. Fang and Y. Zhang, Perfect Nonreciprocal Absorption Based on Metamaterial Slab, *Plasmonics*, 2018, **13**, 661–667.

23 M. Lawrence, D. R. Barton and J. A. Dionne, Nonreciprocal flat optics with silicon metasurfaces, *Nano Lett.*, 2018, **18**, 1104–1109.

24 S. Fang, K. Lua, H. Ma, W. Lv, Y. Li, Z. Zhu, C. Guan, J. Shi and T. Cu, Asymmetric transmission of linearly polarized waves in terahertz chiral metamaterials, *J. Appl. Phys.*, 2017, **121**, 033103.

25 P. Zhang, Q. Leng, Y. Kan, J. Ge and S. Wu, Asymmetric transmission of linearly polarized waves based on chiral metamaterials, *Opt. Commun.*, 2022, **517**, 128321.

26 Z. Ozer, F. Dincer, M. Karaaslan and O. Akgol, Asymmetric transmission of linearly polarized light through dynamic chiral metamaterials in a frequency regime of gigahertz–terahertz, *Opt. Eng.*, 2014, **53**(7), 075109.

27 Y. Huang, Z. Yao, F. Hu, C. Liu, L. Yu, Y. Jin and X. Xu, Tunable circular polarization conversion and asymmetric transmission of planar chiral graphene-metamaterial in terahertz region, *Carbon*, 2017, **119**, 305–313.

28 K. Fang, Z. Yu, V. Liu and S. Fan, Ultracompact nonreciprocal optical isolator based on guided resonance in a magneto-optical photonic crystal slab, *Opt. Lett.*, 2011, **36**, 4254–4256.

29 A. M. Mahmoud, A. Davoyan and N. Engheta, All-passive nonreciprocal metastructure, *Nat. Commun.*, 2015, **6**, 8359.

30 X. Yang, E. Wen and D. Sievenpiper, All-passive microwave-diode nonreciprocal metasurface, *Commun. Phys.*, 2023, **6**, 333.

31 Z. Luo, M. Z. Chen, Z. X. Wang, L. Zhou, Y. B. Li, Q. Cheng, H. F. Ma and T. J. Cui, Digital nonlinear metasurface with customizable nonreciprocity, *Adv. Funct. Mater.*, 2019, **29**, 1906635.

32 J. Zhao, H. Yang, X. Shan, X. Mi, S. Ma and Y. Huang, Research on dual-controlled terahertz metamaterial broadband absorber based on vanadium dioxide and graphene, *Opt. Commun.*, 2023, **545**, 129701.

33 C. Liu, Y. Xu, H. Liu, M. Lin and S. Zha, Switchable metamaterial with terahertz buffering and absorbing performance, *IEEE Photon. J.*, 2021, **13**(5), 1–8.

34 D. Wang, B. Cai, L. Yang, L. Wu, Y. Cheng, F. Chen, H. Luo and X. Li, Transmission/reflection mode switchable ultra-broadband terahertz vanadium dioxide (VO_2) metasurface filter for electromagnetic shielding application, *Surf. Interfaces*, 2024, **49**, 104403.

35 Z. Y. Chen, S. B. Cheng, H. F. Zhang, Z. Yi, B. Tang, J. Chen, J. G. Zhang and C. J. Tang, Ultra wideband absorption absorber based on Dirac semimetallic and graphene metamaterials, *Phys. Lett. A*, 2024, **517**, 129675.

36 Y. Sun, Y. Wang, H. Ye, J. Li, H. Fan, L. Yu, Z. Yu and Y. Liu, Switchable bifunctional metasurface based on VO_2 for ultra-broadband polarization conversion and perfect absorption in same infrared waveband, *Opt. Commun.*, 2022, **503**, 127442.

37 D. Li, S. He, L. Su, H. Du, Y. Tian, Z. Gao, B. Xie and G. Huang, Switchable and tunable terahertz metamaterial absorber based on graphene and vanadium dioxide, *Opt. Mater.*, 2024, **147**, 114655.

38 H. Guan, F. Ren, S. Liang, J. Gu, C. Geng, H. Wei, S. Dou, J. Zhao and Y. Li, Ultra-high transmission broadband tunable VO_2 optical limiter, *Laser Photonics Rev.*, 2023, **17**, 2200653.